A Stable Solid Electrolyte Interphase for Magnesium Metal Anode Evolved from a Bulky Anion Lithium Salt

Kun Tang, Aobing Du, Shanmu Dong, Zili Cui,* Xin Liu, Chenglong Lu, Jingwen Zhao, Xinhong Zhou,* and Guanglei Cui*

Rechargeable magnesium (Mg) metal batteries are a promising candidate for "post-Li-ion batteries" due to their high capacity, high abundance, and most importantly, highly reversible and dendrite-free Mg metal anode. However, the formation of passivating surface film rather than Mg^{2+}-conducting solid electrolyte interphase (SEI) on Mg anode surface has always restricted the development of rechargeable Mg batteries. A stable SEI is constructed on the surface of Mg metal anode by the partial decomposition of a pristine Li electrolyte in the electrochemical process. This Li electrolyte is easily prepared by dissolving lithium tetrakis(hexafluoroisopropyloxy)borate ($Li[B(hfip)_4]$) in dimethoxyethane. It is noteworthy that Mg^{2+} can be directly introduced into this Li electrolyte during the initial electrochemical cycles for in situ forming a hybrid Mg^{2+}/Li^+ electrolyte, and then the cycled electrolyte can conduct Mg-ion smoothly. The existence of this as-formed SEI blocks the further parasitic reaction of Mg metal anode with electrolyte and enables this electrolyte enduring long-term electrochemical cycles stably. This approach of constructing superior SEI on Mg anode surface and exploiting novel Mg electrolyte provides a new avenue for practical application of high-performance rechargeable Mg batteries.

Currently, various rechargeable alkaline or alkaline earth metal (Li, Na, K, Mg) batteries have received extensive concern of researchers owing to the high theoretical specific capacities of these metal anodes.[1] Among these metal anodes, Mg metal is an especially attractive alternative due to its high volumetric capacity (3833 mAh cm^{-3}), resistance to dendrite growth,

abundant resources, environmental amity, and handling safety.[2] The first prototype of rechargeable Mg metal battery has been successfully exploited by Aurbach et al. in 2000, by virtue of the development of Mg organohaloaluminate electrolyte and the employment of Chevrel phase cathode (Mo_6S_8).[3] However, this system is generally known to possess unsatisfactory energy density owing to the low operating voltage ($\approx$1.1 V) and the low specific capacity (80 mAh g^{-1}) of Mo_6S_8 cathode. Since then, tremendous endeavors have been devoted to improving the energy density of rechargeable Mg metal batteries, aimed at exploiting the high-voltage Mg cathode and developing the high-performance Mg electrolytes.[4]

Due to the low reduction potential of Mg metal (−2.37 V vs S.H.E), most electrolyte components are susceptible to be reduced on Mg metal surface, leading to the formation of a solid film covering the Mg anode surface.[5] The current prevailing view is that such surface film generally blocks the reversible Mg plating/stripping and passivates the Mg anode due to the difficult transport of Mg^{2+} in this surface interphase. Hence, many previous investigations on Mg electrolytes mainly focused on synthesizing new Mg salts based on carbanion (such as Grignard reagents) and hydride anions (such as boron-cluster hydrides) that are stable to Mg metal and soluble in ethereal solvent (the only feasible organic solvents currently inert to Mg metal).[4a,e,h,j,6] Those reported Mg electrolyte components, which are strongly reduction-resistant but generally vulnerable oxidation or corrosive, intrinsically limit the possibility of a high-voltage Mg battery operating above 3.0 V.[7] If a Mg^{2+}-conducting solid-electrolyte interphase (SEI) can be formed on the surface of Mg metal anode to hinder the parasitic reaction between electrolyte and anode, it will be possible to decouple the anodic and cathodic requirements for a Mg electrolyte, so that the electrolyte system can support both reversible Mg plating/stripping at the anode side and high-potential intercalations of Mg^{2+} at the cathode side, simultaneously.

Recently, the feasibility of constructing Mg^{2+}-conducting SEI on Mg anode surface has gradually attracted the attention of researchers. Ban et al. engineered an Mg^{2+}-conducting and electronic-insulating artificial interphase on the Mg anode surface, which realized highly reversible Mg chemistry in

K. Tang, Prof. X. Zhou
College of Chemistry and Molecular Engineering
Qingdao University of Science and Technology
No. 53 Zhengzhou Road, Qingdao 266042, China
E-mail: zhouxinhong@qust.edu.cn
A. Du, Dr. S. Dong, Dr. Z. Cui, X. Liu, C. Lu, Dr. J. Zhao, Prof. G. Cui
Qingdao Industrial Energy Storage Research Institute
Qingdao Institute of Bioenergy and Bioprocess Technology
Chinese Academy of Sciences
No. 189 Songling Road, Qingdao 266101, China
E-mail: cuizl@qibebt.ac.cn; cuigl@qibebt.ac.cn
A. Du
Center of Materials Science and Optoelectronics Engineering
University of Chinese Academy of Sciences
No. 19A Yuquan Road, Beijing 100049, China

**ADVANCED
SCIENCE NEWS**

www.advancedsciencenews.com

**ADVANCED
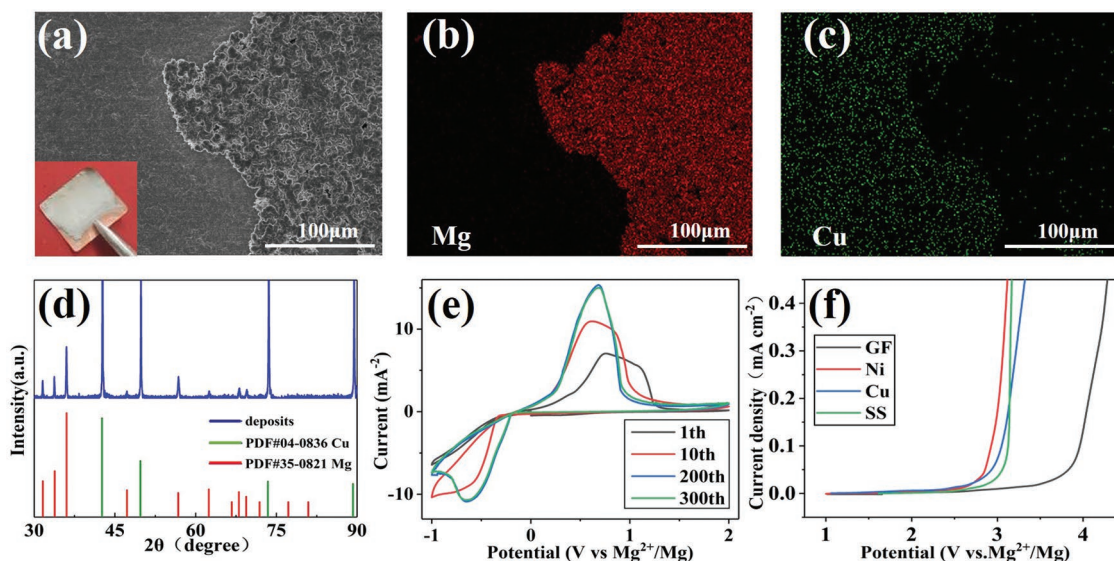MATERIALS**

www.advmat.de

Figure 1. a) Typical SEM images of the deposited Mg on Cu substrate with LBhfip/DME electrolyte. b) Mg, c) Cu EDS element mapping, and d) XRD of the deposits on Cu substrate. e) CV of the Mg/Cu cell (with LBhfip/DME) at a scanning rate of 25.0 mV s^{-1}. f) LSV of LBhfip/DME electrolyte examined with the working electrode of graphite film (GF), Ni, Cu, and SS. The counter and reference electrodes are Mg metal.

oxidation-resistant electrolytes.[7] Cao et al. tailored an inorganic magnesium fluoride (MgF_2) surface layer on Mg anode for improving the performance of full-cell Mg ion batteries.[8] Wang et al. demonstrated that an Mg-ion conductive solid MgI_2 layer could be formed on Mg metal anode surface for acting as a solid electrolyte interface.[9] These observations have challenged the long-held passivation mechanism of Mg/electrolyte interface and verified the possibility of forming SEI on Mg anode surface by some delicate surface modifications. However, there is few report about the direct reduction of Mg electrolyte components for in situ forming an Mg^{2+}-conducting SEI on Mg anode surface.[10]

Tetrakis(hexafluoroisopropyloxy)borate anion (denoted as $B(hfip)_4^-$) based Mg electrolytes have been reported almost simultaneously by our group and Zhao's group, which exhibits superior electrochemical performance, especially in Mg-S battery system.[4e,h,11] However, in this contribution, we have observed that the Mg/Cu asymmetric cell (with $Mg[B(hfip)_4]_2$ based electrolyte, 0.5 M $Mg[B(hfip)_4]_2$ dissolved in dimethoxyethane (DME), abbreviated as MBhfip/DME) cannot sustain the stability in the long cycle charge–discharge process, as shown in Figure S1 (Supporting Information). By sufficient characterizations (Figures S2–S4, Supporting Information), we have detected that MBhfip salt is virtually unstable toward Mg metal anode during the electrochemical cycling and an SEI layer can be formed on Mg anode surface by the partial decomposition of MBhfip salt. Although the SEI formed by decomposed MBhfip salt enables dozens of cycles of reversible Mg plating/stripping in the Mg/Cu asymmetric cell (with MBhfip/DME), this SEI is not very stable that causing poor long-term electrochemical stability. The relevant discussion details about MBhfip/DME electrolyte can be seen in the Supporting Information.

Herein, to improve the cycling stability of $B(hfip)_4^-$ based Mg electrolytes, a pristine Li salt electrolyte (0.5 M $Li[B(hfip)_4]$

dissolved in DME, abbreviated as LBhfip/DME) has been first found that has the ability to plate/strip Mg reversibly and has better cycling stability than above MBhfip/DME electrolyte. First, to strictly illustrate the Mg-ion conducting ability of LBhfip/DME electrolyte, the Mg/Cu asymmetric cell (Mg metal as anode and Cu foil as cathode) with this electrolyte was discharged for 12 h at the current density of 1.0 mA cm^{-2}. The inset of **Figure 1**a displays shiny magnesium deposits on Cu foil substrate. As shown in scanning electron microscopy (SEM) images of Figure 1a and Figure S5 (Supporting Information), the Mg was uniformly deposited, which can be confirmed by the energy-dispersive spectrometry (EDS) mapping results of element Mg and element Cu (Figure 1b,c). Moreover, Figure 1d exhibits that the X-ray diffraction (XRD) result of the deposits only can be indexed to Mg metal and Cu metal, which affirm these deposits are pure Mg metals without any other species. Compared to the deposits in MBhfip/DME electrolyte under the same deposition conditions (Figure S6, Supporting Information), the Mg deposits in LBhfip/DME electrolyte are significantly more uniform and dense. And it is worth noting that the Mg deposits in both two electrolytes have no obvious dendrite formation. Then, the reversible Mg plating/stripping process in LBhfip/DME electrolyte has also indeed been verified by Cyclic voltammogram (CV) tests even for 300 cycles, as shown in Figure 1e. And the linear sweep voltammetry (LSV) results (Figure 1f) indicate that LBhfip/DME has a relative higher anodic stability of ≈2.7 V versus Mg/Mg^{2+} toward Cu, nickel (Ni), and stainless steel (SS) working electrode, which enable this electrolyte matching well with sulfur and Mo_6S_8 cathodes. In addition, as shown in Figure S7 (Supporting Information), the Mg plating/stripping performance of LBhfip salt dissolved into various ether solvents, such as tetrahydrofuran, diethylene glycol dimethyl ether (G2), and triethylene glycol monomethyl ether (G3) solvent have also been investigated by CV measurements. The superior reversibility of Mg plating/stripping in
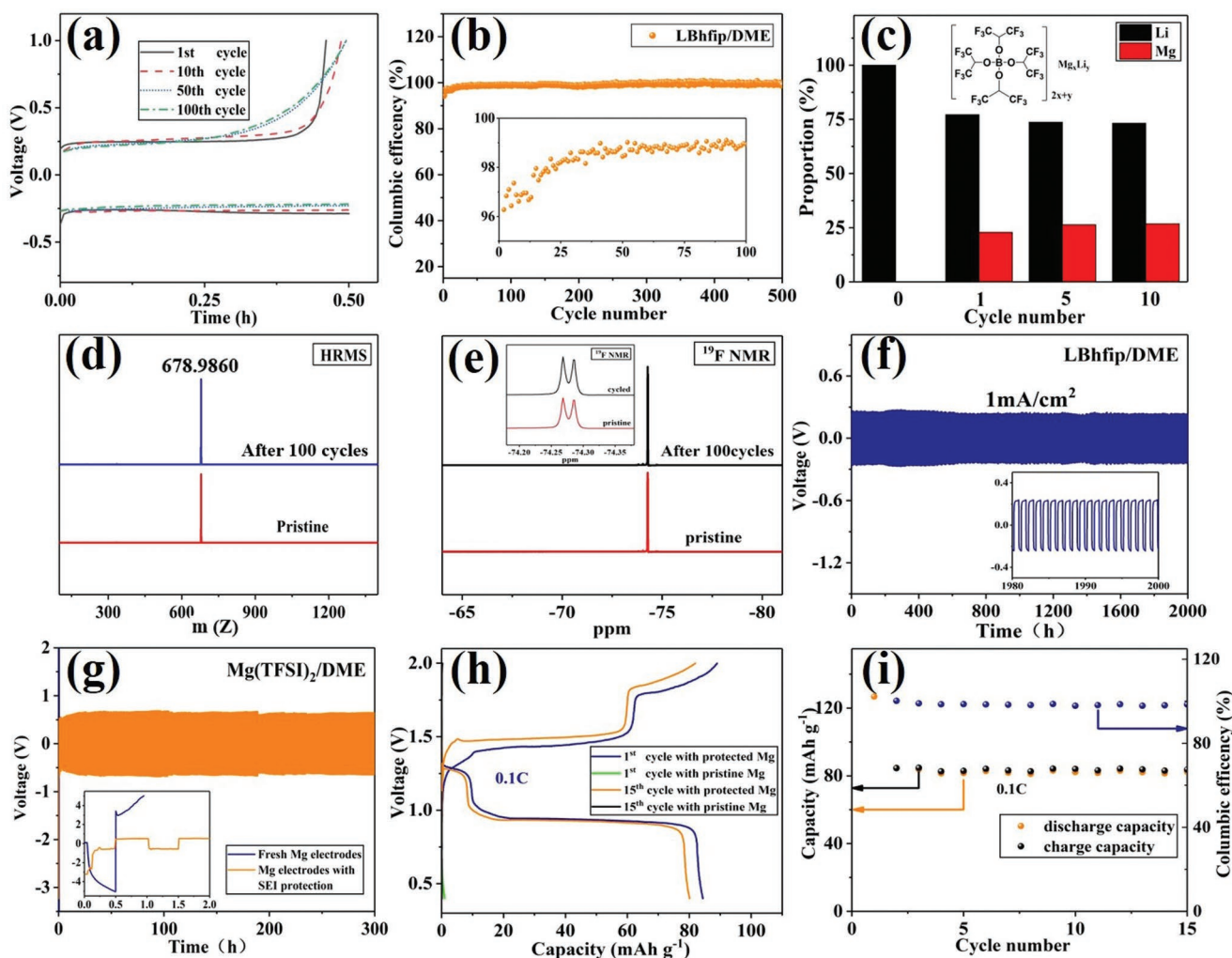
Figure 2. a) Voltage profiles of Mg/Cu cell (with LBhfip/DME) cycled at the charge–discharge current density of 0.5 mA cm^{-2} and b) the corresponding Coulombic efficiency. c) ICP-OES results (the molar proportion of Li element and Mg element) of the LBhfip/DME electrolyte after varied charge–discharge cycles. The comparison of d) HRMS and e) ^{19}F NMR spectra of the LBhfip/DME electrolyte before and after 100 charge–discharge cycles. f) Long-term cycling behavior of the Mg/Mg symmetrical cell (with LBhfip/DME) at the current density of 1.0 mA cm^{-2}. g) Polarization behavior of the Mg/Mg symmetric cell (with bare Mg electrodes) and the Mg/Mg symmetric cell (with SEI protecting Mg electrodes) at the current density of 0.1 mA cm^{-2}, both based on Mg(TFSI)$_2$/DME electrolyte. h) Charge–discharge profiles, i) capacity and Coulombic efficiency of the Mo$_6$S$_8$/Mg batteries (with SEI protecting Mg anode) based on Mg(TFSI)$_2$/DME electrolyte.

these LBhfip/ether systems indicate the wide solvent tolerance of LBhfip salt in Mg electrolytes.

To further evaluate the reversibility of Mg plating/stripping, Mg/Cu asymmetric cell (with LBhfip/DME) has been tested by charging–discharging at the current density of 0.5 mA cm^{-2}, as shown in **Figure 2**a. The corresponding Coulombic efficiency (CE) reaches to 99.0% after 25 activating cycles and can be stably cycled for 500 cycles (Figure 2b), which is better than the cycling stability of the Mg/Cu cell (with MBhfip/DME) (Figure S1c, Supporting Information). Disassembling the Mg/Cu cell (with LBhfip/DME) after 100 charge–discharge cycles, the Mg anode surface has turned gray, and some C, F, and B species are detected on the surface of the cycled Mg anode by EDS analysis, as shown in Figure S8 (Supporting Information). Therefore, the LBhfip/DME electrolyte has been partly decomposed on the Mg anode surface during electrochemical cycling,

and the superior cycling stability can be attributed to the protection of the as-formed stable SEI. In addition, the specific salt components of the cycled LBhfip/DME electrolyte have been identified by various methods including inductively coupled plasma-optical emission spectrometer (ICP-OES), nuclear magnetic resonance (NMR), and high resolution mass spectrometry (HRMS). As shown in Figure 2c, the Mg content in the pristine LBhfip/DME electrolyte is negligible, but after the first cycle, the Mg content in the cycled electrolyte increases and then remains invariant after five cycles. To clearly illustrate what happens on Cu cathode during initial discharge process, the compositional variation of Cu cathode surface at different discharge times have been investigated by XPS and XRD analysis, as shown in Figure S9 (see the Supporting Information for the details). The immediate appearance of Mg^{2+} in the cycled LBhfip/DME electrolyte indicates that Mg^{2+} can be

introduced into this electrolyte as soon as the electrochemical process begins, and then the cycled electrolyte can conduct Mg-ion well. Interestingly, comparing the spectral results (NMR, HRMS) of the pristine LBhfip/DME electrolyte with that of the cycled one, as depicted in Figure 2d,e and Figure S10 (Supporting Information), the decomposed product of Bhfip⁻ anion is not detected in the cycled LBhfip/DME electrolyte, which is completely different from MBhfip/DME electrolyte (Figure S1d,e, Supporting Information). We speculate that those decomposed products of LBhfip/DME electrolyte mostly participate in the formation of SEI on electrode surface, which prevents the further decomposition of the remaining LBhfip/DME well. To estimate the long-term compatibility of LBhfip/DME electrolyte, the Mg/Mg symmetric cell with LBhfip/DME electrolyte has been measured by galvanostatic charge–discharge at the current density of 1.0 mA cm⁻². As shown in Figure 2f, this Mg/Mg symmetric cell can be cycled for 2000 cycles with no significant increase in polarization potential, which indicates LBhfip/DME electrolyte has outstanding long-term stability and superior Mg-ion conductivity. And as shown in Figure S11 (Supporting Information), the electrochemical impedance spectroscopy of Mg/Mg cell after galvanostatic cycling shows a newly generated interface impedance in the high frequency region, which should correspond to the SEI formation on Mg electrode surface.

To further verify the protective effects of this SEI on Mg surface, the cycled Mg electrodes were taken out from the Mg/Mg cells (with LBhfip/DME) to investigate its compatibility with Mg(TFSI)$_2$/DME electrolyte. It is known that Mg(TFSI)$_2$ can chemically react with Mg metal to form passivation layer on the Mg anode surface, which severely hinders its reversible Mg plating/stripping.[12] As shown in Figure 2g, the fresh Mg electrodes experience extremely high and rapidly increased overpotential during galvanostatic cycling in the Mg/Mg symmetric cell with Mg(TFSI)$_2$/DME electrolyte, which is apparently caused by the Mg-surface passivation as a result of reductive decomposition of TFSI⁻ anion. In sharp contrast, the SEI protecting Mg electrodes in the same Mg(TFSI)$_2$/DME electrolyte exhibit excellent reversibility for 300 cycles without pronounced overpotential enhancement, suggesting the superior protective effect of the as-formed SEI. In addition, the anticorrosion properties of the SEI protecting Mg electrode in Mg(TFSI)$_2$/DME electrolyte (measured by the Tafel plot method) is much superior than that of the fresh Mg electrode, as shown in Figure S12 (Supporting Information). Most notably, the SEI protecting Mg anode coupling with Mo$_6$S$_8$ cathode can also operate well with Mg(TFSI)$_2$/DME electrolyte, which should be the first prototype of Mo$_6$S$_8$/Mg battery based on Mg(TFSI)$_2$/DME electrolyte, as shown in Figure 2h,i. In addition to Mg(TFSI)$_2$ salt, propylene carbonat solvent have also been confirmed to be blocked by the as-formed SEI well, as shown in Figure S13 (Supporting Information). These results confirm that a stable SEI layer on Mg anode surface indeed significantly expand the scope of application of practical Mg electrolyte.

To thoroughly investigate the explicit compositions in the stable SEI, the Mg anode surface of the Mg/Cu cell with LBhfip/DME electrolyte after 100 charge–discharge cycles has been analyzed by XPS and time-of-flight secondary ion mass spectrometry

(TOF-SIMS) measurements. As shown in **Figure 3**a–e, the results of B 1s, F 1s, C 1s, O 1s, and Mg 2p XPS spectrum are similar to the cycled Mg anode in MBhfip/DME electrolyte (Figure S4a–e, Supporting Information), which indicates that the SEI formed by LBhfip/DME electrolyte has somehow similar compositions with the forming SEI in MBhfip/DME electrolyte. However, it is worth noting that Li 1s XPS spectrum (Figure 3f) exhibits a significant amount of LiCO$_3$, Li$_2$O, and LiF species located at 55.2, 55.6, and 56.7 eV, respectively.[13] Therefore, these inorganic lithium salts are likely to play a very important role in stabilizing the as-formed SEI on Mg anode surface. TOF-SIMS results (Figure 3g) not only further manifest the presence of Li-containing components in SEI, but also shows that the distribution of SEI components is uniform, which is different from the uneven SEI formed by MBhfip/DME electrolyte (Figure S4f, Supporting Information). In addition to the above comparison of components distribution map, Figure 3h depicts the intensity evolution of various species in the SEI for both electrolytes, as a function of the sputtering time. As the ion sputtering time increases, the signal intensity for O⁻, CO$_3$⁻, and F⁻ species of the SEI formed by LBhfip/DME electrolyte is always higher than that of the SEI formed by MBhfip/DME electrolyte, which indicates the SEI formed by LBhfip/DME electrolyte should be denser. The cross-section SEM images of the Mg anode of the Mg/Cu cell with different electrolytes after 100 charge–discharge cycles have been observed and compared, as shown in Figure 3i. The cycled Mg anode in LBhfip/DME shows an obviously dense and uniform morphology, which indicates that Mg plating/stripping in LBhfip/DME electrolyte should be more homogeneous during the electrochemical charge–discharge process. These results manifest that a stable and dense Li-species-containing SEI could be formed on Mg anode surface based on the reaction between Mg metal and LBhfip/DME, which highly contributes to the reversible Mg plating/stripping. Inspired by the stable Li-species-containing SEI, some Li salts additives (LiNO$_3$, LiPF$_6$) have also been attempted for improving the electrochemical stability of MBhfip/DME electrolyte, which unsuccessfully exhibit reversible Mg plating/stripping behavior (see Figure S14 for the details, Supporting Information). Therefore, the anion species in Mg electrolyte play a crucial role in the formation of stable Li-species-containing SEI on Mg anode surface. Li[B(hfip)$_4$] salt has also been attempted as additive in MBhfip/DME electrolyte (containing 0.5 M Mg[B(hfip)$_4$]$_2$ and 0.2 M Li[B(hfip)$_4$], abbreviated as MLBhfip/DME). As shown in Figure S15 (Supporting Information), the electrochemical stability and reversibility of MLBhfip/DME is significantly better than MBhfip/DME, and slightly worse than LBhfip/DME. The results of XPS and TOF-SIMS (Figure S16, Supporting Information) have also affirmed the existence of Li-species-containing SEI on the cycled Mg anode surface in MLBhfip/DME electrolyte.

Based on the above various experimental analysis, the specific mechanism of SEI formation on Mg anode surface has been first summarized, as illustrated in **Scheme 1**. In MBhfip/DME electrolyte (Scheme 1a), the decomposed products of MBhfip salts participate in forming a loose and unstable SEI on Mg anode surface, thereby causing the Mg anode to be unable to withstand long-cycle electrochemical process. However, in the LBhfip/DME electrolyte (Scheme 1b), Li[B(hfip)$_4$] salts first decompose on the side of low potential and Mg²⁺ enter into
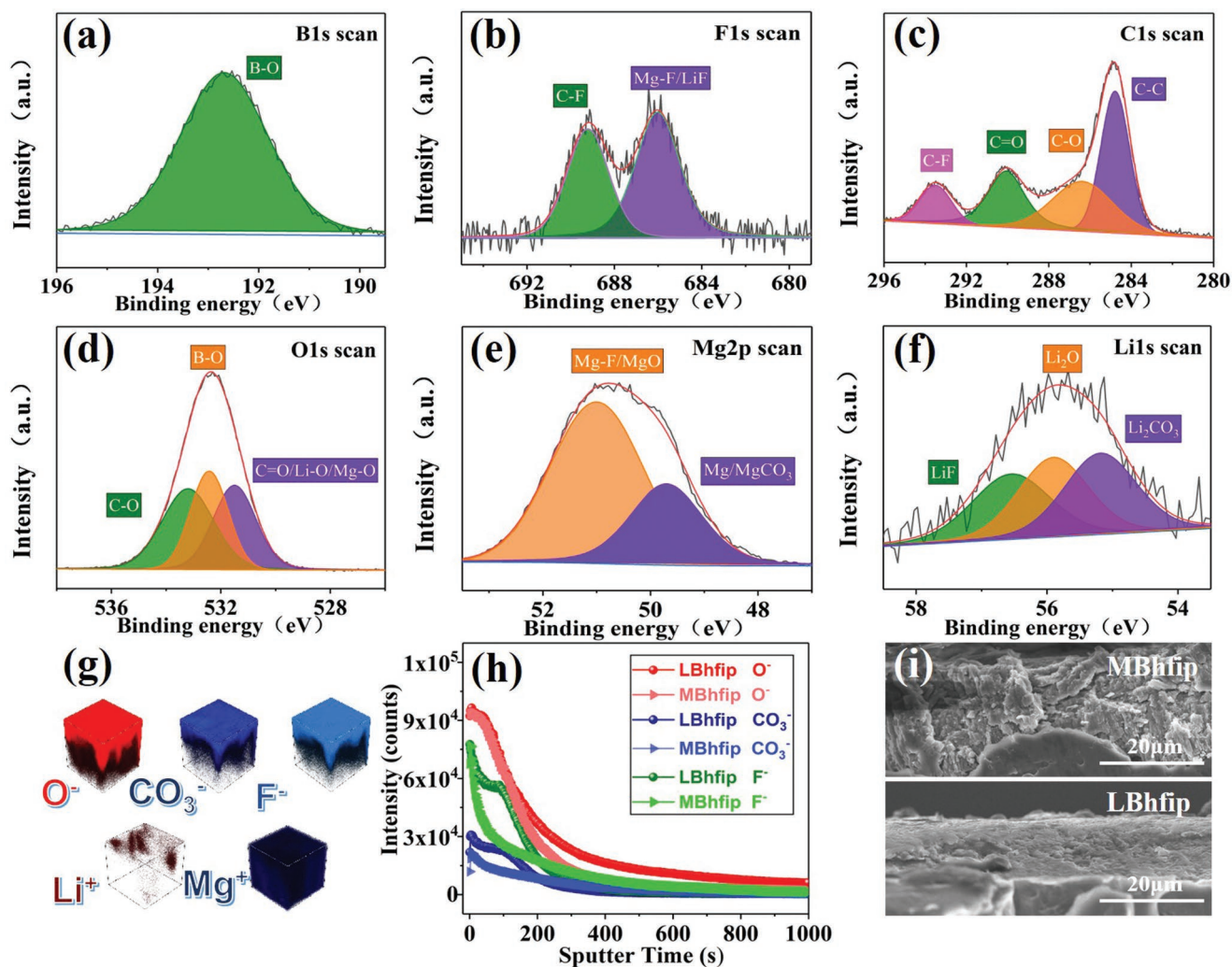
Figure 3. a) B 1s, b) F 1s, c) C 1s, d) O 1s, e) Mg 2p, f) Li1s XPS spectra, and g) TOF-SIMS spectra of O^-, CO_3^-, F^-, Mg^+, Li^+ for the Mg anode surface of the Mg/Cu cell (with LBhfip/DME) after 100 charge–discharge cycles. h) The intensity evolution of O^-, CO_3^-, F^- species as a function of the sputtering time in TOF-SIMS and i) the cross-section SEM images for the cycled Mg anode surface of the Mg/Cu cell (with LBhfip/DME) and the Mg/Cu cell (with MBhfip/DME) after 100 charge–discharge cycles.
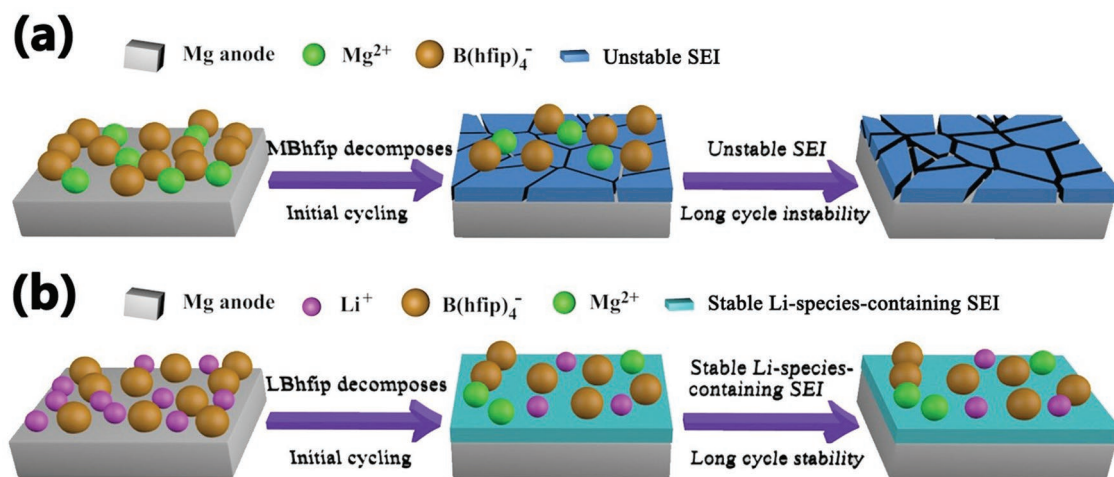
Scheme 1. The specific mechanism of SEI formation on the Mg anode surface in a) MBhfip/DME electrolyte and b) LBhfip/DME electrolyte.
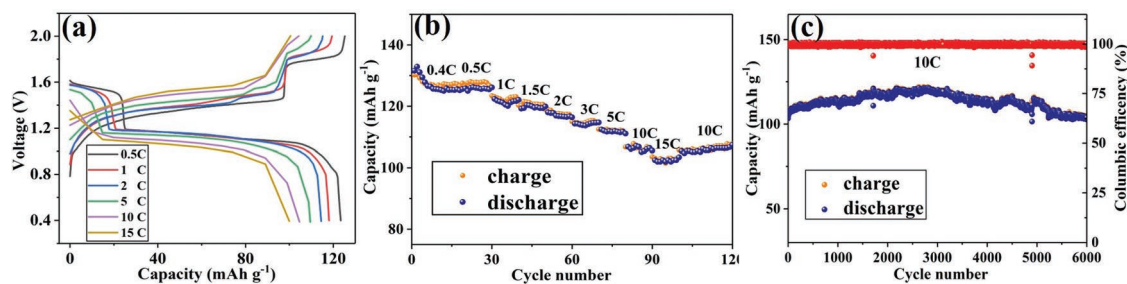
1904987 (5 of 7)

Figure 4. a) Charge–discharge profiles and b) charge–discharge capacity of the Mo_6S_8/Mg battery (with LBhfip/DME electrolyte) at different rates. c) Cycling stability and corresponding Coulombic efficiency of this Mo_6S_8/Mg battery for 6000 cycles at the rate of 10C (1C = 128.8 mA g^{-1}).

the electrolyte from the side of Mg anode during the initial discharge process. After a sufficient amount of Mg^{2+} exists in the electrolyte, LBhfip/DME electrolyte enables Mg^{2+} conduction. After several cycles of charge–discharge, the decomposed products of $Li[B(hfip)_4]$ salt participate in the formation of a stable Li-species-containing SEI on electrode surface, which ensures the reversible and stable Mg plating/stripping during long-cycle electrochemical testing.

To demonstrate the practical application of LBhfip/DME electrolyte in battery system, Mo_6S_8/Mg batteries with this electrolyte have been assembled to investigate its cycling performance. **Figure 4**a,b shows the charge–discharge profiles and specific capacities at different C-rates (1 C = 128.8 mA g^{-1}). The specific capacity decreased slightly as the C-rate increasing, and the discharge capacity still maintains 106.0 mAh g^{-1} even at 15C. The long cycling stability of this Mo_6S_8/Mg battery has also been studied, as shown in Figure 4c. This Mo_6S_8/Mg battery delivers an initial discharge capacity of 100.4 mAh g^{-1} with the Coulomb efficiency of 99.0% at a rate of 10C and the discharge capacity increases gradually to 118.5 mAh g^{-1} after 2800 cycles, which may be due to the slow electrolyte wetting into cathode and the activating process of LBhfip/DME electrolyte. After stable 6000 cycles at 10C, the discharge capacity of this battery is still rather high (101.3 mA g^{-1}), and the average CE over the 6000 cycles is higher than 99.0%. To our knowledge, this is the best performance of the Mo_6S_8/Mg battery that has been reported.[14] In fact, Li^+ intercalation reaction into Mo_6S_8 cathode is the dominant process when both Li^+ and Mg^{2+} are present in the electrolyte simultaneously.[14b,15] Although the above high capacity performance may be due to the reversible intercalation reaction of Li-ion into the Mo_6S_8 cathode, the rate performance and long cycling stability in our LBhfip/DME electrolyte still show impressive advantages.

In conclusion, a stable Li-species-containing SEI could be formed on Mg metal anode surface by the partial decomposition of LBhfip salts in the electrochemical process. Simultaneously, Mg^{2+} can be introduced into this LBhfip/DME electrolyte during the initial electrochemical cycles for in situ forming a hybrid Mg^{2+}/Li^+ electrolyte, and then the cycled LBhfip/DME electrolyte can conduct Mg^{2+} smoothly. The precise species of this cycled LBhfip/DME electrolyte primarily comprises Mg^{2+}, Li^+, and unchanged $B(hfip)_4^-$ anion, which has been confirmed by NMR, ICP-OES, and HRMS. The unchanged $B(hfip)_4^-$ anion in the hybrid Mg^{2+}/Li^+ electrolyte indicate the decomposed products of LBhfip salts mostly precipitate on the Mg anode surface to form Li-species-containing SEI, which can

prevent the further parasitic reaction between the remaining electrolyte and Mg anode. The as-formed Li-species-containing SEI has also been thoroughly analyzed by XPS analysis and TOF-SIMS. This stable SEI highly contributes to reversible Mg plating/stripping in Mg/Cu cell and enables 2000 cycles of stable constant current polarization (1.0 mA cm^{-2}) in Mg/Mg symmetric cell. More importantly, the extracted Mg anodes after cycling in LBhfip/DME electrolyte can be well compatible with $Mg(TFSI)_2/DME$ electrolyte. Notably, the Mo_6S_8/Mg batteries assembled with this LBhfip/DME electrolyte exhibits a discharge capacity of 101.3 mAh g^{-1} after 6000 cycles at the rate of 10C. This ingenious approach of constructing stable SEI by exploiting novel electrolyte provides a promising avenue not only for Mg metal anode but also for other multivalent metal anodes facing the similar problems.

Experimental Section

All experimental details are included in the Supporting Information.

Supporting Information

Supporting Information is available from the Wiley Online Library or from the author.

Conflict of Interest

The authors declare no conflict of interest.

[1] a) J. Muldoon, C. B. Bucur, T. Gregory, *Chem. Rev.* **2014**, *114*, 11683; b) M. Mao, T. Gao, S. Hou, C. Wang, *Chem. Soc. Rev.* **2018**, *47*, 8804.

[2] a) J. Song, E. Sahadeo, M. Noked, S. B. Lee, *J. Phys. Chem. Lett.* **2016**, *7*, 1736; b) P. Canepa, G. Sai Gautam, D. C. Hannah, R. Malik, M. Liu, K. G. Gallagher, K. A. Persson, G. Ceder, *Chem. Rev.* **2017**, *117*, 4287; c) J. Muldoon, C. B. Bucur, T. Gregory, *Angew. Chem., Int. Ed.* **2017**, *56*, 12064.

[3] D. Aurbach, Z. Lu, A. Schechter, Y. Gofer, H. Gizbar, R. Turgeman, Y. Cohen, M. Moshkovich, E. Levi, *Nature* **2000**, *407*, 724.

[4] a) J. Luo, Y. Bi, L. Zhang, X. Zhang, T. L. Liu, *Angew. Chem., Int. Ed.* **2019**, *58*, 6967; b) L. Zhou, Q. Liu, Z. Zhang, K. Zhang, F. Xiong, S. Tan, Q. An, Y. M. Kang, Z. Zhou, L. Mai, *Adv. Mater.* **2018**, *30*, 1801984; c) F. Y. Xiong, Y. Q. Fan, S. S. Tan, L. M. Zhou, Y. A. Xu, C. Y. Pei, Q. Y. An, L. Q. Mai, *Nano Energy* **2018**, *47*, 210; d) Y. Wang, X. Xue, P. Liu, C. Wang, X. Yi, Y. Hu, L. Ma, G. Zhu, R. Chen, T. Chen, J. Ma, J. Liu, Z. Jin, *ACS Nano* **2018**, *12*, 12492; e) Z. Zhao-Karger, M. E. G. Bardaji, O. Fuhr, M. Fichtner, *J. Mater. Chem. A* **2017**, *5*, 10815; f) Z. Zhang, Z. Cui, L. Qiao, J. Guan, H. Xu, X. Wang, P. Hu, H. Du, S. Li, X. Zhou, *Adv. Energy Mater.* **2017**, *7*, 1602055; g) H. D. Yoo, H. Liang, H. Dong, J. Lin, H. Wang, Y. Liu, L. Ma, T. Wu, Y. Li, Q. Ru, Y. Jing, Q. An, W. Zhou, J. Guo, J. Lu, S. T. Pantelides, X. Qian, Y. Yao, *Nat. Commun.* **2017**, *8*, 339; h) A. Du, Z. Zhang, H. Qu, Z. Cui, L. Qiao, L. Wang, J. Chai, T. Lu, S. Dong, T. Dong, H. Xu, X. Zhou, G. Cui, *Energy Environ. Sci.* **2017**, *10*, 2616; i) X. Sun, P. Bonnick, V. Duffort, M. Liu, Z. Rong, K. A. Persson, G. Ceder, L. F. Nazar, *Energy Environ. Sci.* **2016**, *9*, 2273; j) O. Tutusaus, R. Mohtadi, T. S. Arthur, F. Mizuno, E. G. Nelson, Y. V. Sevryugina, *Angew. Chem., Int. Ed.* **2015**, *54*, 7900.

[5] R. Mohtadi, F. Mizuno, *Beilstein J. Nanotechnol.* **2014**, *5*, 1291.

[6] a) J. T. Herb, C. A. Nist-Lund, C. B. Arnold, *ACS Energy Lett.* **2016**, *1*, 1227; b) R. Mohtadi, M. Matsui, T. S. Arthur, S.-J. Hwang, *Angew. Chem., Int. Ed.* **2012**, *51*, 9780.

[7] S.-B. Son, T. Gao, S. P. Harvey, K. X. Steirer, A. Stokes, A. Norman, C. Wang, A. Cresce, K. Xu, C. Ban, *Nat. Chem.* **2018**, *10*, 532.

[8] B. Li, R. Masse, C. Liu, Y. Hu, W. Li, G. Zhang, G. Cao, *Energy Storage Mater.* **2019**, *22*, 96.

[9] X. Li, T. Gao, F. Han, Z. Ma, X. Fan, S. Hou, N. Eidson, W. Li, C. Wang, *Adv. Energy Mater.* **2018**, *8*, 1701728.

[10] R. Attias, M. Salama, B. Hirsch, Y. Goffer, D. Aurbach, *Joule* **2019**, *3*, 27.

[11] Z. Zhao-Karger, R. Liu, W. Dai, Z. Li, T. Diemant, B. Vinayan, C. Bonatto Minella, X. Yu, A. Manthiram, R. J. Behm, *ACS Energy Lett.* **2018**, *3*, 2005.

[12] a) S. Hebie, H. P. K. Ngo, J. C. Lepretre, C. Iojoiu, L. Cointeaux, R. Berthelot, F. Alloin, *ACS Appl. Mater. Interfaces* **2017**, *9*, 28377; b) S. Hebié, F. Alloin, C. Iojoiu, R. Berthelot, J.-C. Leprêtre, *ACS Appl. Mater. Interfaces* **2018**, *10*, 5527.

[13] a) J. Contour, A. Salesse, M. Froment, M. Garreau, J. Thevenin, D. Warin, *J. Microsc. Spectrosc. Electron.* **1979**, *4*, 483; b) K. Hamrin, G. Johansson, U. Gelius, C. Nordling, K. Siegbahn, *Phys. Scr.* **1970**, *1*, 277.

[14] a) Y. Shao, T. Liu, G. Li, M. Gu, Z. Nie, M. Engelhard, J. Xiao, D. Lv, C. Wang, J.-G. Zhang, *Sci. Rep.* **2013**, *3*, 3130; b) Y. Cheng, Y. Shao, J.-G. Zhang, V. L. Sprenkle, J. Liu, G. Li, *Chem. Commun.* **2014**, *50*, 9644; c) Y. Cheng, H. J. Chang, H. Dong, D. Choi, V. L. Sprenkle, J. Liu, Y. Yao, G. Li, *J. Mater. Res.* **2016**, *31*, 3125.

[15] M. Levi, E. Lancry, H. Gizbar, Z. Lu, E. Levi, Y. Gofer, D. Aurbach, *J. Electrochem. Soc.* **2004**, *151*, A1044.